Inorganic Chemistry

Article

pubs.acs.org/IC

Quantitative Analysis of Deconvolved X-ray Absorption Near-Edge Structure Spectra: A Tool To Push the Limits of the X-ray Absorption Spectroscopy Technique

Paola D'Angelo,*[,†] Valentina Migliorati,[†] Ingmar Persson,[‡] Giordano Mancini,[§,⊥] and Stefano Della Longa[∥]

[†]Dipartimento di Chimica, Università di Roma "La Sapienza", P. le A. Moro 5, 00185 Rome, Italy

[‡]Department of Chemistry and Biotechnology, Swedish University of Agricultural Sciences, P.O. Box 7015, SE-750 07 Uppsala, Sweden

[§]Scuola Normale Superiore, Piazza dei Cavalieri 7, I-56126 Pisa, Italy

[⊥]Istituto Nazionale di Fisica Nucleare (INFN) Sezione di Pisa, Largo Bruno Pontecorvo 3, I-56127 Pisa, Italy

[∥]Dipartimento di Medicina Clinica, Sanità Pubblica, Scienze della Vita e dell'Ambiente, Università dell'Aquila, I-67100 L'Aquila, Italy

ABSTRACT: A deconvolution procedure has been applied to K-edge X-ray absorption near-edge structure (XANES) spectra of lanthanoid-containing solid systems, namely, hexakis-(dmpu)praseodymium(III) and -gadolinium(III) iodide. The K-edges of lanthanoids cover the energy range 38 (La)−65 (Lu) keV, and the large widths of the core-hole states lead to broadening of spectral features, reducing the content of structural information that can be extracted from the raw X-ray absorption spectra. Here, we demonstrate that deconvolution procedures allow one to remove most of the instrumental and core-hole lifetime broadening in the K-edge XANES spectra of lanthanoid compounds, highlighting structural features that are lost in the raw data. We show that quantitative analysis of the deconvolved K-edge XANES spectra can be profitably used to gain a complete local structural characterization of lanthanoid-containing systems not only for the nearest neighbor atoms but also for higher-distance coordination shells.

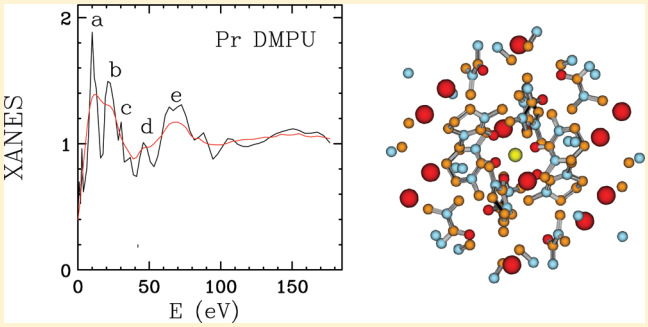

1. INTRODUCTION

X-ray absorption spectroscopy (XAS) is one of the most widely used experimental techniques to study the electronic and spatial structure of materials.[1−15] XAS spectra of condensed systems are broadened with respect to the ideal signal due to intrinsic and instrumental effects. Intrinsic broadening highly affects XAS measurements of elements absorbing at high energies, more than 30 keV where the core-hole lifetime $\tau_{corehole}$ is very short. Then, the experimental spectrum is the convolution of the ideal signal with a Lorentzian having full width at half-maximum (fwhm) of $\Gamma_c = \hbar/\tau_{corehole}$. Modern facilities for XAS experiments allow one to collect high-quality spectra characterized by low noise and high resolution. As a result, present day spectra contain much more information than previous ones, but this cannot be appreciated due to the presence of core-hole lifetime broadening. In order to retrieve all of the information contained in the XAS spectra, various deconvolution procedures mainly focused on Fourier-based techniques have been developed. Loffen et al.[16] found that one can remove approximately half of the lifetime broadening using Wiener filtering. Babanov et al.[17] developed a deconvolution algorithm based on the regularization of an ill-posed inverse problem leading to an iterative procedure. Klementev suggested an improved deconvolution method using a Bayesian approach which incorporates X-ray photoemission results as prior information.[18] Fister et al.[19] proposed the use of the Richardson-Lucy iterative algorithm as a method for deconvolving instrumental and intrinsic resolution from typical XAS data. Filipponi developed an algorithm based on the convolution theorem in Fourier space, and he found that one can remove about two-third of the lifetime broadening by using a Gaussian filter.[20]

In parallel with the development of deconvolution procedures, novel experimental methods to measure X-ray-absorption spectra with a reduced inner-shell lifetime broadening have been proposed. In the pivotal work by Hämäläinen et al.,[21] a high-resolution spectrometer has been used to analyze the fluorescence photon energy at the Dy L_3-edge with better resolution than the natural line width. More recently, the resonant inelastic X-ray scattering (RIXS) technique has been developed that is based on a two-step process separated into a resonant excitation to an intermediate state and a subsequent decay into a final state.[22,23] In RIXS spectroscopy as in

Received: June 10, 2014
Published: August 29, 2014

   dx.doi.org/10.1021/ic501366d | *Inorg. Chem.* 2014, 53, 9778−9784

conventional X-ray absorption near-edge structure (XANES), the density of the lowest unoccupied states is probed, but absorption features are better resolved.[22,23]

Even if several deconvolution procedures have been developed in the past, deconvolved XANES signals have been hardly analyzed on a quantitative ground. Only a few examples are reported in the literature. An unexpected 7-fold coordination of the hydrated Hg^{2+} complex in aqueous solution has been revealed from the quantitative analysis of a deconvolved Hg L_3-edge spectrum.[24,25] The structural properties of the hydrated lanthanoid(III) ions in aqueous and dimethyl sulfoxide (DMSO) solutions have been investigated by analyzing the deconvolved lanthanoid K-edge XANES signals.[26−28]

In this paper, the focus is on the use of a deconvolution procedure to highlight structural features in K-edge XANES spectra of lanthanoid-containing compounds in the solid state. When dealing with heavy elements, the K-edge transitions occur at high energy, and the spectra are strongly broadened due to the short core-hole lifetime. In the case of solid samples, the core-hole effect makes it impossible to detect distant shells from the analysis of the extended X-ray absorption fine structure (EXAFS) signal. Here, it is demonstrated that the quantitative XANES analysis of deconvolved spectra of elements of higher atomic number allows one to gain structural information also for more distant coordination shells in solid samples. In particular, the coordination chemistry of *N*,*N*′-dimethylpropyleneurea, dmpu, solvated Pr^{3+} and Gd^{3+} ions in solid state has been explored by XANES at the K-edge. The MXAN method[29,30] has been used to quantitatively reproduce the XANES spectra, and the additional features obtained from the deconvolution procedures are well reproduced by theoretical calculations. The results of the present study demonstrate that K-edge XANES spectra at high energy can be successfully used to gain a complete local structural characterization of such systems also beyond the first coordination sphere.

The present analysis has been carried out on solid samples of known structure in order to prove the efficiency of the analysis procedure; however, this approach can be used also to determine the coordination geometry in systems of unknown structure. In this context, the coordination structure of lanthanoid(III) ions in solution or in disordered systems can be unraveled through the cooperation of deconvolution procedure and MXAN analysis. This combined approach can provide unique information on lanthanoid-containing systems both in solution and solid state that can hardly be obtained from other experimental techniques.

2. EXPERIMENTAL SECTION

2.1. Materials and XAS Data Collection. Crystalline hexakis(dmpu)praseodymium(III) iodide and hexakis-(dmpu)gadolinium-(III) iodide were prepared as described in ref 31; the structure of dmpu is given in Figure 1.

Pr and Gd K-edge XAS spectra were collected at the bending magnet beamline BM23,[32] at the European Synchrotron Radiation Facility (ESRF), in transmission geometry. The storage ring was operating in 16-bunch mode with a typical current of 80 mA after refill. The spectra were collected using a Si(511) double crystal monochromator with the second crystal detuned by 20% for harmonic rejection. The intensity of the X-ray beam was measured by three consecutive ionization chambers filled with Kr/He gas mixture. The sample cell was inserted between the first pair of chambers, and Pr or Gd foils between the last pair, for energy calibration. The spectra were calibrated by assigning the first inflection point of the Pr and Gd foil spectra to 41991 and 50239 eV, respectively. The samples were diluted with boron nitride to give an absorption change over the edge of about one logarithmic unit. The spectra were recorded in a wide range from 41.0 and 49.23 keV for Pr and Gd, respectively, with a 5 eV spacing refining to a minimum of 0.2 eV in the edge and then increasing again with $\delta k = 0.02$ Å^{-1}. For each sample, three scans were averaged, giving an averaged final spectrum that was used in the data analysis.

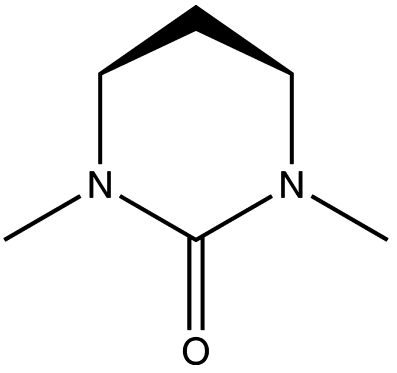

Figure 1. Structure formula of *N*,*N*′-dimethylpropyleneurea, dmpu, where the middle propylene carbon atom lies out of the plane. For purposes of clarity, hydrogen atoms have been omitted.

2.2. XANES Data Analysis. The analysis of the XANES data was carried out with the MXAN code.[30] MXAN uses the muffin tin (MT) approximation for the shape of the potential and a complex optical potential, based on the local density approximation of the self-energy of the excited photoelectron. The MT radii have been chosen on the basis of previous investigations and are 1.7 Å for praseodymium and gadolinium, 0.8 Å for oxygen, 0.9 Å for carbon, and 0.7 Å for nitrogen.[28] The self-energy is calculated in the framework of the Hedin-Lundqvist (HL) scheme. Inelastic losses are accounted for by MXAN using a phenomenological approach on the basis of a convolution of the theoretical spectrum. Only the real part of the HL potential is used in the calculation, with a Lorentzian function having an energy-dependent width of the form $\Gamma_{tot}(E) = \Gamma_c + \Gamma_{mfp}(E)$. The constant part, Γ_c, includes the core-hole lifetime, while the energy-dependent term, $\Gamma_{mfp}(E)$, represents all the intrinsic and extrinsic inelastic processes. The function $\Gamma_{mfp}(E)$ is zero below an onset energy, E_s, and begins to increase from a value, A_s, following the universal functional form of the mean free path in solids. Both the onset energy E_s and the jump A_s are introduced in the Γ_{tot}(E) function via an arctangent functional to avoid discontinuities and to simulate the electron−hole pair excitations. Their numerical values are derived at each computational step (i.e., for each geometric configuration) on the basis of a Monte Carlo fit. The experimental resolution is taken into account by a Gaussian convolution. The minimization procedures have been carried out starting from the X-ray structures of hexakis(dmpu)praseodymium(III) and hexakis(dmpu)gadolinium(III) iodide.[33] Least-squares fits of the experimental data in the space of the structural and nonstructural parameters are achieved by minimizing the residual function defined as

$$R_{sq} = \frac{\sum_{i=1}^{m} w_i (y_i^{th} - y_i^{exp})^2}{\varepsilon_i^2 \sum_{i=1}^{m} w_i} \quad (1)$$

where m is the number of data points, y_i^{th} and y_i^{exp} are the theoretical and experimental values of absorption, respectively, ε_i is the individual error in the experimental data set, and w_i is a statistical weight. For w_i = constant = 1, the square residual function, R_{sq}, becomes the statistical χ^2 function. Here, we assumed a constant experimental error, $\varepsilon = 1.2\%$, for the whole experimental data set. The structural parameters were the Ln−O, Ln−C, and Ln−N distances reported in Table 1, while the orientation of the dmpu ligands has been kept fixed to the crystallographic geometry.

dx.doi.org/10.1021/ic501366d | Inorg. Chem. 2014, 53, 9778−9784

Table 1. Ln−O, Ln−CO, Ln−CH_3, and Ln−N Distances As Determined from the Crystallographic Structure for Hexakis (dmpu)praseodymium(III) Iodide and Hexakis (dmpu)gadolinium(III) Iodide[33]

	N	*R* (Å)
$[Pr(dmpu)_6]^{3+}$ crystal structure	6 O	2.34
	6 CO	3.56
	6 CH_3	4.19
	6 N	4.33
	6 N	4.42
	6 CH_3	4.43
$[Gd(dmpu)_6]^{3+}$ crystal structure	6 O	2.27
	6 CO	3.51
	6 CH_3	4.17
	2 CH_3	4.22
	4 CH_3	4.28
	10 N	4.32
	2 N	4.37

3. RESULTS

3.1. Deconvolution of High-Energy K-Edge X-ray Absorption Spectra. In core−shell X-ray spectroscopy, the measured spectra are degraded with respect to the ideal signal due to the combined effects of intrinsic and experimental broadening. The effect is particularly dramatic when dealing with K-edge spectra of heavy elements. As mentioned in the introduction, deconvolution methods can be applied to XANES data that largely facilitate the detection of spectral features and the comparison with theoretical calculations. We applied the deconvolution procedure developed by Filipponi[20] to the Pr and Gd K-edge XAS spectra of solid hexakis(dmpu)-praseodymium(III) and -gadolinium(III)iodide using the DECONV program that is part of the GNXAS package.[34,35]

In particular, the deconvolution of a Lorentzian function of width Γ_c is performed by applying a direct Fourier transformation on the measured absorption spectrum $\alpha(E)$ in the energy space

$$\tilde{\alpha}(q) = \int_{-\infty}^{\infty} \exp(iqE)\alpha(E)\, dE \quad (2)$$

In the method developed by Filipponi[20] instead of interpolating the measured spectrum on a uniform energy mesh and to use the fast Fourier transform algorithm, the original spectrum with a variable energy spacing is used, and the Fourier integral is calculated numerically. All details of this procedure can be found in ref 20. The deconvolution of a Lorentzian broadening of width Γ_c is then performed in Fourier space by

$$\tilde{\alpha}_D(q) = \tilde{\alpha}(q) \exp(\Gamma_c|q)\omega(q) \quad (3)$$

where $\omega(q)$ is a suitable window function, while $\tilde{\alpha}_D(q)$ actually corresponds to the spectrum resulting from the deconvolution of the Lorentzian width Γ_c and the convolution by a function corresponding to the back Fourier transform of the window function. The deconvolved function of eq 3 has then to be back transformed to direct space.[20] The complete deconvolution of the core-hole broadening is achieved by putting $\omega(q) = 1$, but this is not possible due to the noise blow-up effect. As a consequence, a Gaussian filter with full width at half-maximum σ is adopted, and the minimum σ that can be used is limited by the noise blow-up effect. In a typical case where the noise level is on the order of 10^{-4}, the corresponding minimum σ value is $\sigma = \Gamma_c/3$. However, for spectra having a higher noise level, reasonable values of σ are in the range $\Gamma_c/3 < \sigma < \Gamma_c/2$. The optimal σ can be chosen on a case-by-case basis by selecting the lowest value that does not give rise to ringing artifacts in the deconvolved spectrum, and its value clearly depends on the quality of the original spectrum. The possibility to convert the Lorentzian resonance into a much narrower Gaussian peak is at the basis of the good results of the deconvolution procedure.

In the present case, the core-hole widths (fwhm) at the K-edge are Γ_c = 16.2 and 22.3 eV for praseodymium and gadolinium, respectively,[36] and the deconvolution procedure has been carried out by deconvolving the entire Γ_c values and applying Gaussian filters with σ values of 6.4 and 10.0 eV for Pr and Gd, respectively. These values have been chosen according to the previously mentioned criterion. The deconvolved spectra are shown in Figure 2 together with the raw data. Clearly, the oscillatory structure in the deconvolved spectra is better resolved, and some new features have emerged from shoulders in the original spectra. In particular, the features a, b, c, d, and e are reported in Figure 2 that are smeared out in the experimental spectrum. In the case of Gd only, the features a, b, d, and e are extracted, whereas there is no evidence of feature c. These features are reproduced by the theoretical calculation as it will be shown below. It is important to stress that the amplitude of the deconvolved signals observed in Figure 2 is mainly related to the Gaussian filter used in the deconvolution procedure, and no physical information can be derived from it.

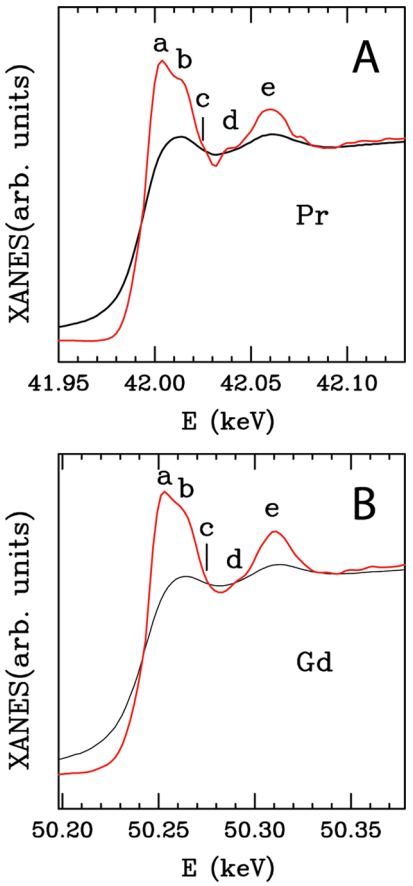

Figure 2. Comparison between the raw K-edge (black line) and deconvolved (red line) XANES spectra of $[Pr(dmpu)_6]^{3+}$ (A) and $[Gd(dmpu)_6]^{3+}$ (B) complexes.

dx.doi.org/10.1021/ic501366d | Inorg. Chem. 2014, 53, 9778−9784

Note that use of the deconvolution procedure allows one to extract additional structural and electronic features from the XANES spectra at the K-edge for systems absorbing at high energy (30 keV or more). This is very useful as the theoretical framework for the analysis of the K-edge XANES spectra is well established, while the quantitative analysis of the XANES data at the L-edges can be more challenging. In particular, XAS investigations on lanthanoid(III) ions in aqueous solution have shown the presence of double-electron excitation channels at the L-edges of these elements that make the quantitative analysis very difficult due to the presence of nonstructural sharp features in the spectra.[37−43] Also the K-edge spectra of lanthanoid-containing systems show the presence of double-electron excitation edges, but in this case they do not alter the XANES data as in the case of the L-edge spectra.[26]

3.2. Theoretical Analysis of XANES Spectra. In order to determine to what extent the deconvolution procedure has been able to recover structural information from the XANES data, a quantitative analysis of the spectra has been carried out.

The theoretical XANES features arise as multiple scattering contributions from a cluster of atoms around the photoabsorber: starting from the crystallographic structure of the $[Pr(dmpu)_6]^{3+}$ and $[Gd(dmpu)_6]^{3+}$ complexes[33] it is possible to calculate the theoretical XANES spectra as a function of the cluster size. In the crystallographic structures, the praseodymium(III) and gadolinium(III) ions are coordinated by six dmpu molecules arranged in an octahedral fashion with six oxygen atoms of the carbonyl group in the first shell, with Pr−O and Gd−O distances of 2.34 and 2.26 Å, respectively. The second shell is formed by the six carbonyl carbon atoms, while the third shell comprises six additional carbon atoms belonging to the methyl groups.

The XANES calculations as a function of the cluster size are shown in Figures 3 and 4 for Pr and Gd, respectively, where the cutoff distances from bottom to top (3.6, 4.2, 5.5, and 10.0 Å) correspond to the inclusion of 2, 3, 4, and 7 coordination shells, respectively. The corresponding atomic clusters considered in the calculations are depicted at right in Figures 3 and 4. In these figures, the theoretical spectra are reported without convolution with the broadening function (see the XANES data analysis section), while the theory vs experiment fit is done after convolving the spectra with a Lorentzian function having an energy-dependent width $\Gamma_{tot}(E)$. It is evident from inspection of the spectra in Figures 3 and 4 that the calculations as a function of the cluster size converge at a cutoff distance of about 5.5 Å. When the cluster size is enlarged from 5.5 to 10.0 Å the peaks become sharper but no additional features arise. Conversely, when only two shells are included in the calculation (cutoff = 3.6 Å), features c and d are completely missing. Feature c comes out only when the methyl carbon atoms are included, while feature d is originated by the inclusion of all of the nitrogen atoms and both methyl groups. According to these observations, the cluster we have chosen to perform the quantitative fit of the broadening terms in the XANES spectrum consists of four coordination shells up to 5.5 Å; more distant atoms are not included to minimize the computational cost.

In Figure 5, the theoretical spectra obtained with a distance cutoff of 10 Å (without broadening) are compared to the deconvolved experimental spectra of $[Pr(dmpu)_6]^{3+}$ and $[Gd(dmpu)_6]^{3+}$ complexes, respectively. As it is evident from a visual inspection of the figures, the spectral features a, b, c, and d that emerge only after deconvolution of the experimental

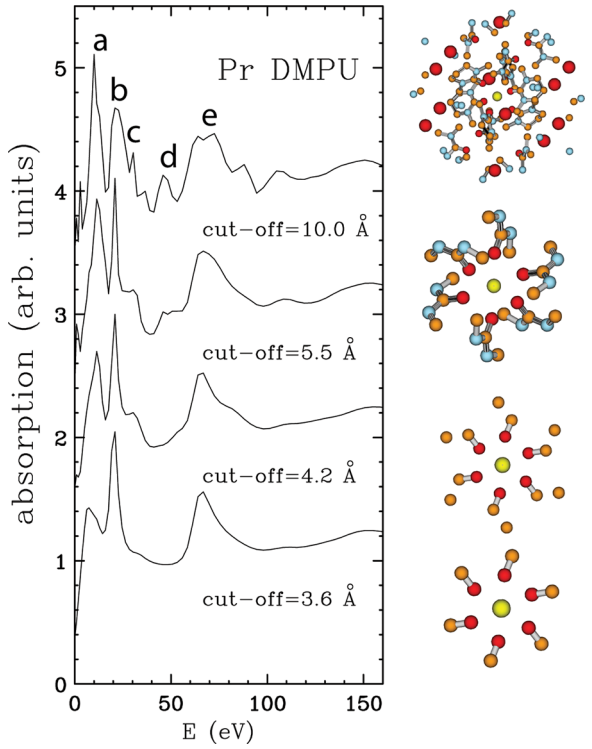

Figure 3. Simulated XANES spectra of the $[Pr(dmpu)_6]^{3+}$ complex as a function of the cutoff radii used in the calculations. The spectra do not include the broadening function. The atomic clusters used in the calculations are also depicted where the praseodymium, oxygen, nitrogen, and carbon atoms are in yellow, red, cyan, and orange, respectively.

spectra well match the corresponding sharp features of the theoretical calculations. These findings prove on the one hand that the deconvolution procedure is able to correctly extract the structural features from the experimental spectra, and on the other that K-edge XANES spectra at very high energy can be successfully used to gain structural information at longer distances.

In the last step of this study, a quantitative analysis of the deconvolved K-edge XANES spectra of solid hexakis(dmpu)-praseodymium(III) and -gadolinium(III) iodide has been carried out, with the aim of assessing the potentiality of high-energy XANES in elucidating the coordination geometry of lanthanoid-containing systems having a medium-range order. Thus, the MXAN procedure has been applied starting from the crystallographic structures[33] and including four coordination shells in the theoretical calculations. During the minimization the Ln−O, Ln−CO, Ln−N, and Ln−CH_3 crystallographic distances listed in Table 1 were optimized, and a variation of less than 2% has been found for all the structural refined parameters. The statistical errors on the refined structural parameters were found in the range 0.03−0.05 Å. In addition, six nonstructural parameters have been optimized, namely, the Fermi energy level E_F, the threshold energy E_0, and energy E_s and amplitude A_s of the plasmon. The theoretical signal is then convoluted by both a Lorentian and Gaussian functions having full width at half-maximum equal to Γ_{res} and Γ_{gau}, respectively. These parameters have a different meaning as compared to the standard MXAN analysis previously described, as in the present case we are fitting a deconvolved spectrum and not the raw data. In particular, Γ_{res} is a residual Lorentian broadening that is

dx.doi.org/10.1021/ic501366d | Inorg. Chem. 2014, 53, 9778−9784

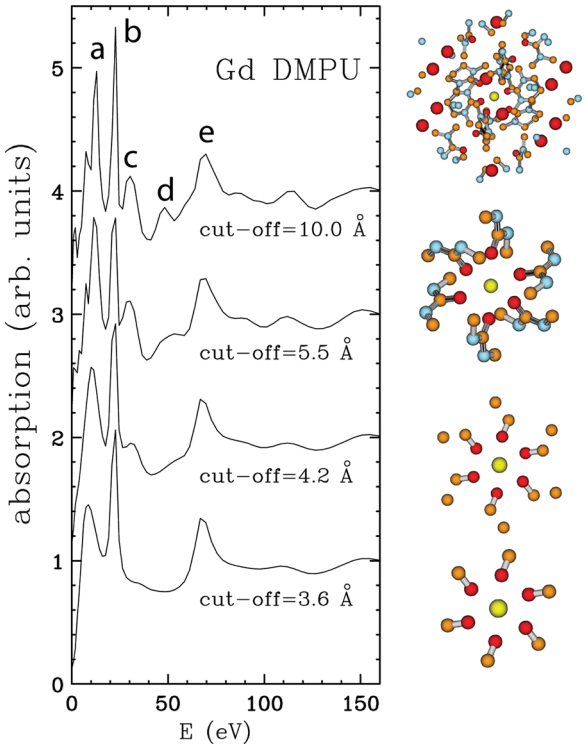

Figure 4. Simulated XANES spectra of the $[Gd(dmpu)_6]^{3+}$ complex as a function of the cutoff radii used in the calculations. The spectra do not include the broadening function. The atomic clusters used in the calculations are also depicted where the gadolinium, oxygen, nitrogen, and carbon atoms are in yellow, red, cyan, and orange, respectively.

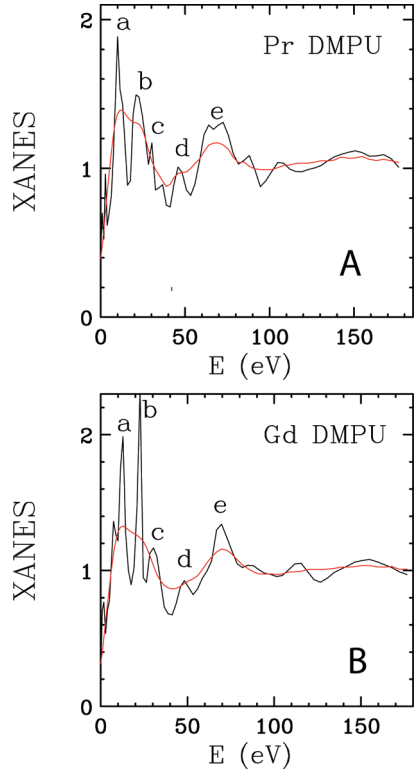

Figure 5. Comparison between the K-edge deconvolved XANES spectra (red line) and the theoretical signal not including the broadening function calculated with a cutoff distance of 10.0 Å (black line) of $[Pr(dmpu)_6]^{3+}$ (A) and $[Gd(dmpu)_6]^{3+}$ (B) complexes.

needed to better model the electron mean free path, while Γ_{gau} accounts for both the experimental resolution and the width of the Gaussian filter used in the deconvolution procedure. A full list of the refined parameters is reported in Table 2. Note that

Table 2. Nonstructural Parameters Obtained from the Minimization Procedures[a]

	E_F (eV)	E_0 (eV)	E_s (eV)	A_s	Γ_{res} (eV)	Γ_{gau} (eV)
Pr(III)	−0.9	41992.0	41.0	10.0	3.5	4.4
Gd(III)	−3.2	50240.5	21.7	5.0	4.3	8.4

[a] E_F is the Fermi energy level with respect to the threshold energy, E_0 is the threshold energy, E_s and A_s are the energy and amplitude of the plasmon, respectively, Γ_{res} is a residual Lorentian broadening and Γ_{gau} is the width of the Gaussian convolution function accounting for both the experimental resolution and the width of the Gaussian filter used in the deconvolution procedure.

the Γ_{gau} values are in reasonable agreement with the width of the Gaussian filter used in the deconvolution procedure. Anyhow, it is important to stress that no physical meaning can be ascribed to the Γ_{res} and Γ_{gau} parameters as they are used to reproduce the amplitude of the deconvolved spectrum that depends mainly on the width of the Gaussian filter used in the deconvolution and, as a consequence, is strongly related to the quality of the original experimental data.

The results of the fitting procedures are shown in Figure 6, for Pr(III) and Gd(III), where the experimental deconvolved spectra are shown together with the best-fit theoretical curves. The comparison shows an excellent agreement between theory and experiment suggesting that the overall procedure tested in

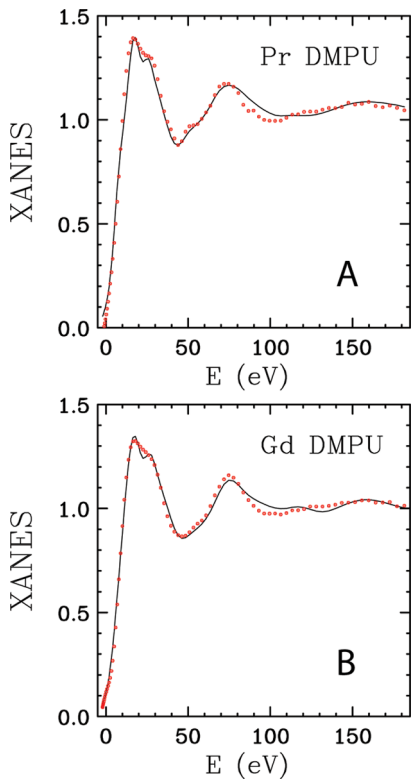

Figure 6. Comparison of the deconvolved K-edge XANES experimental spectra (red dotted line) of $[Pr(dmpu)_6]^{3+}$ (A) and $[Gd(dmpu)_6]^{3+}$ (B) complexes and the best-fit theoretical spectra (black solid line).

dx.doi.org/10.1021/ic501366d | Inorg. Chem. 2014, 53, 9778−9784

the present work, i.e., deconvolution of experimental XANES spectra plus MXAN fit, can be really efficient to provide structural information beyond the first coordination shell from the analysis of their K-edge spectra.

3.3. Discussion and Conclusions. We have measured XANES spectra at the K-edge of crystalline hexakis(dmpu)-praseodymium(III) and hexakis (dmpu)gadolinium(III) iodide. As the K-edge transitions of lanthanoid atoms occur at high energy, the core-hole lifetime broadening strongly damps the spectra, and, in particular, it affects the high frequency components of the measured signals. This clearly reduces the sensitivity of the XAS technique to the longer range interatomic distances. Here, we demonstrate that if high-quality XANES data are collected this lost information can be recovered by applying a proper deconvolution procedure, thus highlighting the contribution associated with higher-distance coordination shells in solid systems. Moreover, we show that K-edge XANES spectra at very high energy (30 keV or more) can be profitably analyzed on a quantitative ground and can be used to extract complete structural information on the system. It is important to stress that high-energy XANES investigations at the K-edge offer advantages over corresponding L-edges due to the lower influence of intense resonance peaks and multielectron excitation processes. In this context, deconvolution can offer a viable strategy, with respect to the full analysis in the RIXS plane that certainly provides a full picture of the excitation/radiative-decay processes, if the objective is only to obtain better resolved spectra.

In this work, the validity of the deconvolution procedure has been assessed by comparing the deconvolved XANES spectra with theoretical calculations carried out on solid samples of known structure; however, this approach can be used also to unravel the coordination geometry in systems of unknown structure. In this context, starting from the results of the present work we are carrying out a further study of lanthanoid ions in liquid dmpu solutions with the aim of accurately determining the three-dimensional structure of the coordination complexes. In fact, in solution the lanthanoid ions have been found to have a coordination geometry that differs from the one present in the solid phase.[33] As it is well-known that it is very difficult to determine the coordination geometry of ions in disordered systems, the deconvolved K-edge XANES spectra can provide unique information that can hardly be obtained from other experimental techniques. Application of deconvolution procedures also can be very useful for lower energy K-edge XANES spectra. In this case it is possible to highlight spectral features occurring in the edge region that are strictly related to the electronic and geometric structure of absorbing centers, thus increasing the content of information that can be extracted from the experimental data.

The results of this investigation pave the route for the use of deconvolved XANES spectra to extract quantitative structural information on systems containing heavy elements.

AUTHOR INFORMATION

Corresponding Author

*E-mail: p.dangelo@uniroma1.it.

Notes

The authors declare no competing financial interest.

ACKNOWLEDGMENTS

We acknowledge the European Synchrotron Radiation Facility for provision of synchrotron radiation facilities and we would like to thank the staff of BM23 for assistance in using the beamline. This work was supported by the University of Rome "La Sapienza" (Progetto ateneo 2013, No. C26A13K8AN) (PD), by the CINECA supercomputing centers through the grant IscrC_COLACIL (n.HP10CCQEUQ) (V.M., P.D.), and by the Swedish Research Council (I.P.).

REFERENCES

(1) Rehr, J. J.; Albers, R. C. *Rev. Mod. Phys.* **2000**, *72*, 621−654.
(2) Filipponi, A.; Ottaviano, L.; Passacantando, M.; Picozzi, P.; Santucci, S. *Phys. Rev. E* **1993**, *48*, 4575.
(3) Diaz-Moreno, S.; Munoz-Paez, A.; Chaboy, J. *J. Phys. Chem. A* **2000**, *104*, 1278.
(4) Migliorati, V.; Mancini, G.; Tatoli, S.; Zitolo, A.; Filipponi, A.; De Panfilis, S.; Di Cicco, A.; D'Angelo, P. *Inorg. Chem.* **2013**, *52*, 1141−1150.
(5) Migliorati, V.; Zitolo, A.; Chillemi, G.; D'Angelo, P. *ChemPlusChem* **2012**, *77*, 234−239.
(6) Mancini, G.; Sanna, N.; Barone, V.; Migliorati, V.; D'Angelo, P.; Chillemi, G. *J. Phys. Chem. B* **2008**, *112*, 4694−4702.
(7) D'Angelo, P.; Migliorati, V.; Mancini, G.; Chillemi, G. *J. Phys. Chem. A* **2008**, *112*, 11833−11841.
(8) D'Angelo, P.; Zitolo, A.; Migliorati, V.; Mancini, G.; Persson, I.; Chillemi, G. *Inorg. Chem.* **2009**, *48*, 10239−10248.
(9) Chillemi, G.; Barone, V.; D'Angelo, P.; Mancini, G.; Persson, I.; Sanna, N. *J. Phys. Chem. B* **2005**, *109*, 9186−9193.
(10) Burattini, E.; D'Angelo, P.; Giglio, E.; Pavel, N. V. *J. Phys. Chem.* **1991**, *95*, 7880−7886.
(11) Mino, L.; Agostini, G.; Borfecchia, E.; Gianolio, D.; Piovano, A.; Gallo, E.; Lamberti, C. *J. Phys. D: Appl. Phys.* **2013**, *46*, 423001.
(12) Bordiga, S.; Groppo, E.; Agostini, G.; van Bokhoven, J. A.; Lamberti, C. *Chem. Rev.* **2013**, *113*, 1736−1850.
(13) Frenkel, A. I. *Chem. Soc. Rev.* **2012**, *41*, 8163−8178.
(14) Singh, J.; Lamberti, C.; van Bokhoven, J. A. *Chem. Soc. Rev.* **2010**, *39*, 4754−4766.
(15) Russell, A. E.; Rose, A. *Chem. Rev.* **2004**, *104*, 4613−4636.
(16) Loeffen, P. W.; Pettifer, R. F.; Müllender, S.; van Veenendaal, M. A.; Röhler, J.; Sivia, D. S. *Phys. Rev. B* **1996**, *54*, 14877−14880.
(17) Babanov, Y.; Ryazhkin, A.; Sidorenko, A.; Blaginina, L. *Nucl. Instrum. Methods Phys. Res. A* **1998**, *405*, 378−381.
(18) Klementev, K. V. *J. Phys. D* **2001**, *34*, 2241.
(19) Fister, T. T.; Seidler, G. T.; Rehr, J. J.; Kas, J. J.; Elam, W. T.; Cross, J. O.; Nagle, K. P. *Phys. Rev. B* **2007**, *75*, 174106.
(20) Filipponi, A. *J. Phys. B: At. Mol. Opt. Phys.* **2000**, *33*, 2835−2846.
(21) Hämäläinen, K.; Siddons, D. P.; Hastings, J. B.; Berman, L. E. *Phys. Rev. Lett.* **1991**, *67*, 2850−2853.
(22) Glatzel, P.; Bergmann, U. *Coord. Chem. Rev.* **2005**, *249*, 65−95.
(23) Glatzel, P.; Sikora, M.; Fernández-García, M. *Eur. Phys. J. Special Topics* **2009**, *169*, 207−214.
(24) Chillemi, G.; Mancini, G.; Sanna, N.; Barone, V.; Della Longa, S.; Benfatto, M.; Pavel, N. V.; D'Angelo, P. *J. Am. Chem. Soc.* **2007**, *129*, 5430−5436.
(25) D'Angelo, P.; Migliorati, V.; Mancini, G.; Barone, V.; Chillemi, G. *J. Chem. Phys.* **2008**, *128*, 084502.
(26) D'Angelo, P.; De Panfilis, S.; Filipponi, A.; Persson, I. *Chem.—Eur. J.* **2008**, *14*, 3045−3055.
(27) D'Angelo, P.; Zitolo, A.; Migliorati, V.; Persson, I. *Chem.—Eur. J.* **2010**, *16*, 684−692.
(28) D'Angelo, P.; Migliorati, V.; Spezia, R.; De Panfilis, S.; Persson, I.; Zitolo, A. *Phys. Chem. Chem. Phys.* **2013**, *15*, 8684−8691.
(29) Benfatto, M.; Della Longa, S. *J. Synchrotron Radiat.* **2001**, *8*, 1087.
(30) Benfatto, M.; Della Longa, S.; Natoli, C. R. *J. Synchrotron Radiat.* **2003**, *10*, 51−57.

(31) Abbasi, A.; Damian Risberg, E.; Eriksson, L.; Mink, J.; Persson, I.; Sandström, M.; Sidorov, Y. V.; Skripkin, M. Y.; Ullström, A.-S. *Inorg. Chem.* **2007**, *46*, 7731−7741.
(32) Filipponi, A.; Borowski, M.; Bowron, D. T.; Ansell, S.; Panfilis, S. D.; Di Cicco, A.; Itiè, J.-P. *Rev. Sci. Instrum.* **2000**, *71*, 2422−2432.
(33) Lundberg, D.; Persson, I.; Eriksson, L.; D'Angelo, P.; De Panfilis, S. *Inorg. Chem.* **2010**, *49*, 4420−4432.
(34) Filipponi, A.; Di Cicco, A.; Natoli, C. R. *Phys. Rev. B* **1995**, *52*, 15122−15134.
(35) Filipponi, A.; Di Cicco, A. *Phys. Rev. B* **1995**, *52*, 15135−15149.
(36) Krause, M. O.; Oliver, J. H. *J. Phys. Chem. Ref. Data* **1979**, *8*, 329−338.
(37) Kodre, A.; Arcon, I.; Hribar, M.; Stuhec, M.; Villain, F.; Drube, W.; Tröger, L. *Physica B* **1995**, *208*, 379−380.
(38) Solera, J. A.; Garc a, J.; Proietti, M. G. *Phys. Rev. B* **1995**, *208*, 2678−2686.
(39) Yamaguchi, T.; Nomura, M.; Wakita, H.; Ohtaki, H. *J. Chem. Phys.* **1988**, *89*, 5153−5159.
(40) Bénazeth, S.; Purans, J.; Chalbot, M.-C.; Kim Nguyen-van Duong, M.; Nicolas, L.; Keller, F.; Gaudemer, A. *Inorg. Chem.* **1998**, *37*, 3667−3674.
(41) Lindqvist-Reis, P.; Lamble, K.; Pattanik, S.; Persson, I.; Sandström, M. *J. Phys. Chem. B* **2000**, *104*, 402−408.
(42) Chaboy, J.; García, J.; Marcelli, A.; Ruiz-López, M. R. *Chem. Phys. Lett.* **1990**, *174*, 389−395.
(43) Chaboy, J.; Tyson, T. A. *Phys. Rev. B* **1994**, *49*, 5869−5875.